SOFT ROBOTICS

Optoelectronically innervated soft prosthetic hand via stretchable optical waveguides

Huichan Zhao,[1] Kevin O'Brien,[1] Shuo Li,[2] Robert F. Shepherd[1]*

Because of their continuous and natural motion, fluidically powered soft actuators have shown potential in a range of robotic applications, including prosthetics and orthotics. Despite these advantages, robots using these actuators require stretchable sensors that can be embedded in their bodies for sophisticated functions. Presently, stretchable sensors usually rely on the electrical properties of materials and composites for measuring a signal; many of these sensors suffer from hysteresis, fabrication complexity, chemical safety and environmental instability, and material incompatibility with soft actuators. Many of these issues are solved if the optical properties of materials are used for signal transduction. We report the use of stretchable optical waveguides for strain sensing in a prosthetic hand. These optoelectronic strain sensors are easy to fabricate, are chemically inert, and demonstrate low hysteresis and high precision in their output signals. As a demonstration of their potential, the photonic strain sensors were used as curvature, elongation, and force sensors integrated into a fiber-reinforced soft prosthetic hand. The optoelectronically innervated prosthetic hand was used to conduct various active sensation experiments inspired by the capabilities of a real hand. Our final demonstration used the prosthesis to feel the shape and softness of three tomatoes and select the ripe one.

INTRODUCTION

Human hands serve not only prehensile functions but also as powerful sensory organs (*1*): We feel the world by the sense of touch, mostly through our hands. Hence, the loss of a hand not only means losing the ability of grasping and manipulation but also closes a door to sensory perception—hand amputees can no longer touch and feel through their fingers. Therefore, an ideal prosthetic hand should achieve dexterous manipulation as well as rich sensation (*2*). Fortunately, many kinds of brain-computer interfaces are being developed to realize the direct communication between human brain and external devices (*3*–*5*), and the effectiveness of using feedback sensation to enhance the functionality of prosthetic hands has been demonstrated by other researchers through patient-involved experiments (*6*, *7*). The work presented here is focused on increasing sensation in a soft and dexterous prosthetic hand.

Advanced prosthetic hands have realized dexterous motions by increasing the degrees of freedom (DOFs) (*8*, *9*) or by using underactuated mechanisms (*10*–*13*). Most of these hand prosthetic systems are powered by motors (*2*, *8*, *10*–*13*). Recently, fluidically powered soft actuators have shown their potential in prosthetics and orthotics (*14*–*16*); these devices, compared with their motor-driven counterparts, are lighter, undergo continuous and more natural deformation with simple control inputs (*17*, *18*), are easy to fabricate (*14*, *19*), and, because of their liquid phase processing, are more likely to be realized in mass production (e.g., replica molding, injection molding, and rotational molding) (*20*, *21*). However, very few soft prosthetics have demonstrated equivalent sensing ability as motor-driven hand prosthetics, which often achieve proprioceptive sensing through motor motion encoders (*8*, *10*–*13*) and realize force sensing through multiaxial force/torque load cells (*10*, *12*, *13*), which are bulky and rigid. In contrast, fluidically driven soft systems operate via stretching of their bodies at strains, $\epsilon = (L - L_0)/L_0 > 0.50$ (*14*, *19*, *22*). Most existing sensors are incompatible with these large strains, and although efforts are being made to develop stretchable sensors for soft actuators (*23*–*29*), there is still an opportunity for reliable, easy-to-fabricate, safe, and chemically stable ones.

We report the use of stretchable optical waveguides for strain sensing in a prosthetic hand. These photonic strain sensors are easy to fabricate, are chemically inert, and demonstrate low hysteresis and high precision in their output signals. As a demonstration of their potential, we used them as curvature, elongation, and force sensors integrated into a fiber-reinforced soft prosthetic hand. We used this optoelectronically innervated prosthetic hand to conduct various active sensation experiments inspired by the capabilities of a real hand.

RESULTS

Stretchable sensors based on waveguides

In the early 1970s, by deforming an elastomeric cladding, Xerox Corporation patented an optical waveguide modulator (*30*). In the 1980s, elastomeric waveguides were used in strain sensing (*31*), tactile sensing (*32*), position sensing (*33*), acoustic sensing (*34*), and gas sensing (*35*); however, the fabrication of these sensors usually required complex instruments and processes and could only be achieved by large corporations and national laboratories. Since the 1990s, because of newly available fabrication techniques [e.g., soft lithography (*36*)], elastomeric waveguides have been applied as innovative sensors in academic research (*37*, *38*). We have developed a class of these sensors—elastomeric optical waveguides—and applied them to prosthetics.

This waveguide is fabricated to be intentionally lossy—as light propagates through it, some radiates to the environment, and the more it is deformed, the more light is lost. We measure the light power loss of the waveguide using a photodetector to indicate its deformation. Specifically, the sensory waveguide is a step-index multimode optical fiber composed of a core with a high refractive index ($n_{core} \sim 1.46$) that has a cross-sectional area (A_{core}) of about 1 mm × 1 mm and clad with an elastomer that has a lower refractive index ($n_{clad} \sim 1.40$) with a cross-sectional area (A_{clad}) of about 3 mm × 3 mm. To fabricate the stretchable waveguide, we use a four-step soft lithography process (*39*) (Fig. 1A): (i) three-dimensionally print (3D-print hereinafter) a mold

[1]Sibley School of Mechanical and Aerospace Engineering, Cornell University, Ithaca, NY 14853, USA. [2]Department of Materials Science and Engineering, Cornell University, Ithaca, NY 14853, USA.
*Corresponding author. Email: rfs247@cornell.edu

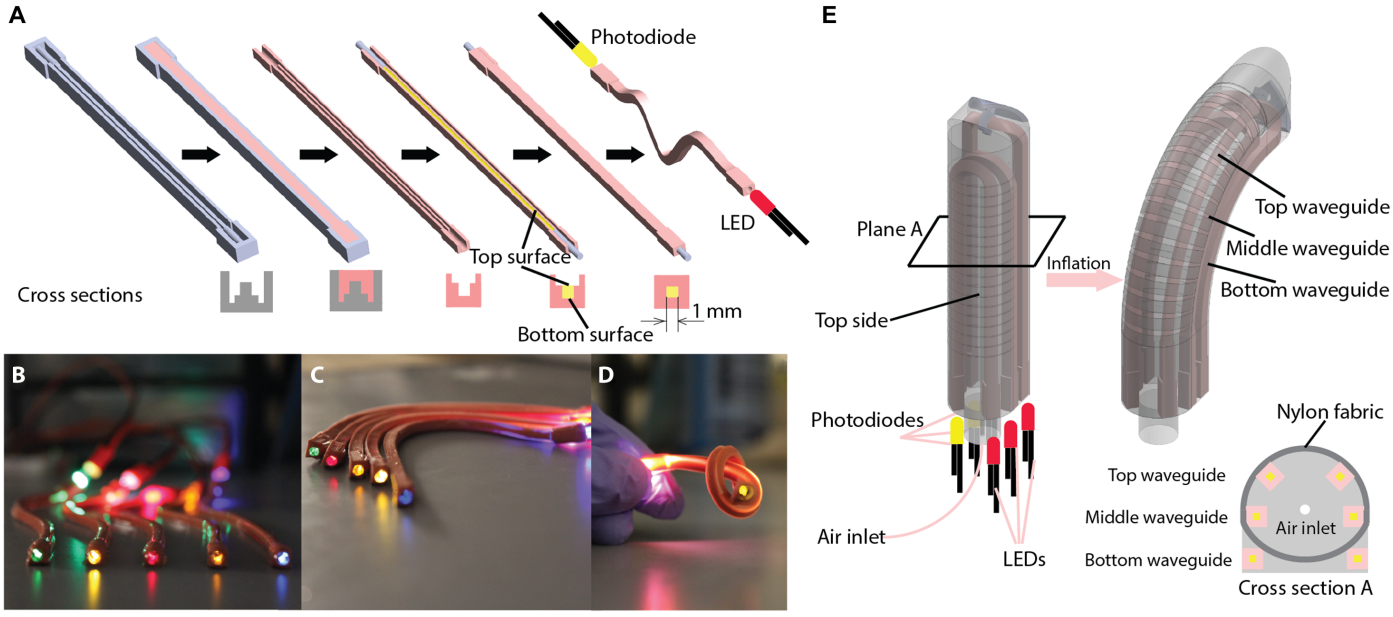

Fig. 1. Stretchable waveguide fabrication and structure of the optoelectronically innervated soft finger. (**A**) Steps for fabricating a waveguide and the corresponding cross section for each step; (**B**) fabricated waveguides with LEDs of assorted colors inserted from one end in a sinuous shape; (**C**) waveguides in a curved shape; (**D**) waveguide in a knot; (**E**) schematic of a soft innervated finger in both unpowered (left) and powered (right) states and its cross section (bottom right corner).

to make the cladding, (ii) pour a pre-elastomer for the cladding into the mold and demold after curing, (iii) fill the cladding with the pre-elastomer of the core material, and (iv) pour the pre-elastomers of the cladding to enclose the core. We also cast two holes at each end of the waveguide to house the light-emitting diode (LED) and the photodetector (i.e., the photodiode). Soft lithography ensures that all structures of the initial mold are replicated in the final waveguide without any loss of detail, including surface roughness (*40*).

The core material of the waveguide is a transparent polyurethane rubber (VytaFlex 20, Smooth-On Inc.) with an n_{core} = 1.461 and a propagation loss of 2 dB/cm at a wavelength of 860 nm, and the cladding material is a highly absorptive silicone composite (ELASTOSIL M 4601 A/B, Wacker Chemie AG) with an n_{clad} = 1.389 and a propagation loss of 1500 dB/cm at a wavelength of 860 nm. The optical properties for these two materials over a larger wavelength range (400 to 1000 nm) are shown in fig. S1 (A and B). Because of the relatively large difference in n for the elastomers, the numerical aperture (NA = 0.45 at 860 nm) ensures a large acceptance angle (θ_{max} ~ 26°) of light input and thus lowers the coupling difficulties for the LED and the photodetector at the extent of the waveguide.

The resulting waveguide is different from commercial ones for several reasons:

(1) It is highly compliant and stretchable. The core and cladding materials have ultimate elongations, ϵ_{ult} ~ 10 and ϵ_{ult} ~ 7, respectively, and elastic moduli (measured at 100% strain), E' ~ 300 kPa and E' ~ 400 kPa, respectively (fig. S2). The combination of high compliance and extensibility allows these waveguides to operate as bending, elongation, and pressure sensors for most situations a hand would typically encounter (e.g., pressing, touching, and grasping).

(2) The core material has a relatively large propagation loss compared with those used for fiber-optic communication. Because our waveguides are applied to prosthetic hands for sensation, this relatively large propagation loss improves sensitivity during elongation while still allowing a detectable amount of light over the length scales typical of a human hand using a low-cost photodiode and a simple current amplifying circuit.

(3) Our cladding material absorbs light at a rate of 1500 dB/cm. This low-index material serves not only as the cladding to ensure total internal reflection for light inside the waveguide but also as the jacket to protect the core, and forms the coupling house for the LED and the photodetector, preventing ambient light from altering the signal.

(4) We 3D-print the molds using a PolyJet printer (Objet30) for our optical waveguides. This fabrication process generates a surface roughness of 6 nm between the core and cladding [root mean square (RMS); see fig. S3]. This relatively rough interface causes scattering and thus more loss of propagation; however, the design freedom of 3D printing allows for complex sensor shapes.

After the waveguides are fabricated, we cast three of them into a finger actuator using overmolding (Fig. 1E). The body of the finger is made of silicone elastomer (Ecoflex 00-30, Smooth-On Inc.), whose optical and mechanical properties are shown in figs. S1 and S2. The 3D integration of the sensors and actuators means that the waveguides are parts of the body and they will deform when the actuator does, serving as proprioceptive sensors.

Characterization of waveguide sensors

We define the output power of a waveguide with no bending, no elongation, and no pressing deformation as the baseline power I_0. With the output power as I, the output power loss in decibels is then defined as

$$a = 10 \log_{10}(I_0/I)$$

By this definition, the output power loss compared to the baseline is always 0, with increasing power $a < 0$ and decreasing power $a > 0$.

To characterize the sensitivity of the waveguides during different deformation modes, we measured the output power of a length

of stretchable waveguide during (i) elongation, (ii) bending, and (iii) pressing (see fig. S4 for characterization methods).

Elongation

For the elongation data (Fig. 2A), we observed a highly linear response curve of power loss with strain. This linear curve can be derived from the Beer-Lambert law

$$A = eLc$$

where A is absorbance, L is the path length, e is the absorptivity of the material, and c is the concentration of chemical species in the medium that attenuate light. Assume constant e and c while stretching, A is proportional to L, and by definition of A

$$A = \log_{10}(I_0/I) + b = a/10 + b$$

where b is the baseline absorbance. Strain is defined as

$$\epsilon = (L - L_0)/L_0$$

so that

$$a = 10ecL_0\epsilon$$

and $10ecL_0$ is a constant.

Experimental results using a waveguide with L_0 = 100 mm yielded a linear, stretch-dependent loss of about 2 dB/cm over $\Delta\epsilon \sim 0.85$ with an LED (peak wavelength ~ 875 nm; TSHA4400, Vishay Intertechnology Inc.) and a photodiode (380 to 1100 nm; SFH 229, OSRAM Licht AG); using different input power, light frequency, or photodetector parameters will alter this sensitivity. Therefore, it is important to calibrate the waveguides accordingly. In addition to linearity, the waveguide, when operating as a stretch sensor, also shows high repeatability (see fig. S5A and movie S1), high precision, and a high signal-to-noise ratio (50 to 150; Fig. 2, error bars indicate noise) over the tested range.

Bending

The waveguide we developed has anisotropic optical transmission properties (Fig. 2B). The "top" of the waveguide core interface (indicated in Fig. 1A) is atomically smooth, whereas the "bottom" core interface has an RMS roughness of 6 nm due to demolding from a 3D-printed surface (fig. S3). The result of this anisotropy is that the signal output depends on the direction of bending: Bending toward the top surface (i.e., the top is in compression and the bottom is in tension) leads to a signal rise followed by a drop in output power, whereas bending toward the bottom surface causes the output power to decrease monotonically. Using this difference, we can determine whether the sensor is being bent up or down. There is no anisotropy in bending side to side (although future versions could be programmed with this feature).

In addition to directional anisotropy, the optical transmission loss rate depends on curvature (*41*). To characterize this dependence, we measured the power output during bending at a uniform curvature of up to $\kappa \sim 200\ m^{-1}$. The output power loss versus κ shows a linear trend in the medium curvature range of 20 to 70 m^{-1} and a sensitivity of 0.02 dB·m cm^{-1}. We note that, although the sensing profile is nonlinear, it is highly repeatable and precise (movie S2) and thus easy to calibrate.

Pressing

Because of the low elastic moduli of our constituent elastomers, small forces exerted over the area of a fingertip can cause a large local deformation in the waveguide. We used this property to sense pressing and tested the power output response to varying forces exerted externally. Our results show that acute pressing (e.g., $\Delta A < 6\ mm^2$) causes a linear response in output power; however, blunt pressing (e.g., $\Delta A > 15\ mm^2$) results in a nonlinear response (Fig. 2C). These results mean that we can change the sensitivity of the waveguide by changing its dimensions to fit the working range of a particular application. The repeatability of pressing sensation is demonstrated in movie S3 and fig. S5B.

This compliant, stretchable waveguide shares the same material library (including silicone elastomers, polyurethane elastomers, and tough hydrogels) as that of many commonly developed soft robots (*19*, *21*, *42*). It shows high linearity to elongation, bending, and local pressing and is highly repeatable and precise. To demonstrate the capability of these waveguides for imparting sensation to soft robots, we incorporated them into the fingers of a soft prosthetic hand.

Innervated prosthetic hand design

Our prosthetic hand is composed of four pneumatically actuated soft fingers and a thumb mounted onto a 3D-printed rigid palm (Fig. 3A). Each digit is a hollow silicone tube (outer diameter, 18 mm; inner diameter, 1 mm; Fig. 1E) with fibers patterned into the elastomer.

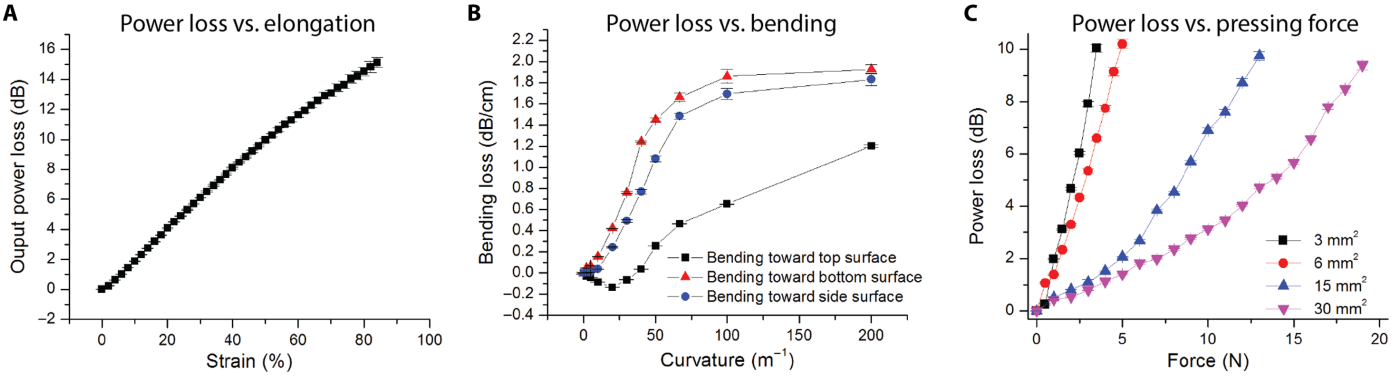

Fig. 2. Characterization of the waveguide sensor in different deformation modes. Characterization for (**A**) pure elongation, (**B**) pure bending, and (**C**) pure pressing. (Error bars indicate SEs from 20 cyclic tests of one waveguide sample).

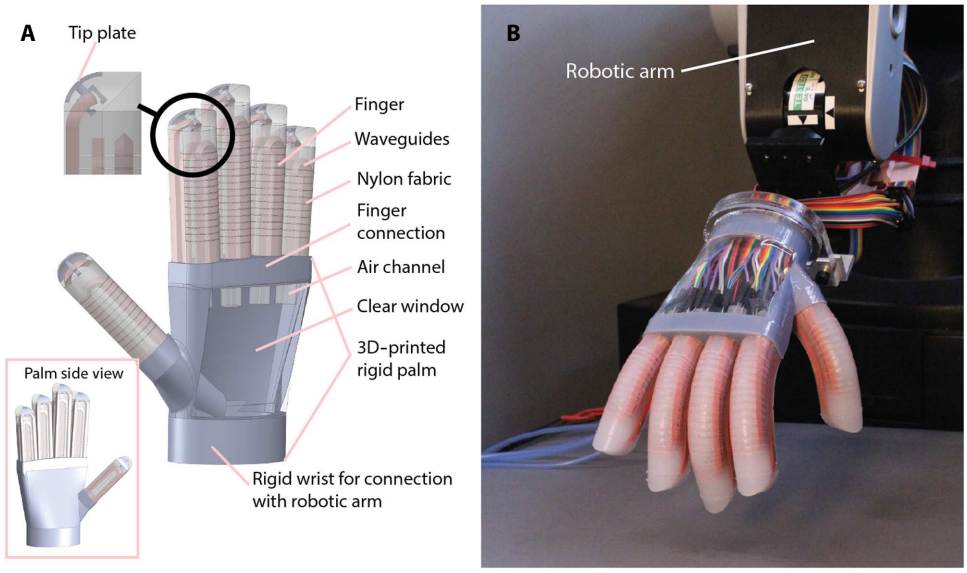

Fig. 3. Innervated prosthetic hand. (**A**) Schematic of hand structure and components; (**B**) image of the fabricated hand mounted on a robotic arm with each finger actuated at ΔP = 100 kPa.

Compressed air enters each finger through their hollow cores and the inflation pressure causes the fingers to bend and the hand to grasp.

Actuation

We patterned the fabric in the actuator to cause a finger-like motion upon pressurization. The nylon fabric is laser-cut to be solid on one side and to have slits on the other. This design is based on a mechanical model we previously established, where constraining circumferential stretching during inflation causes more axial actuation and the strain-limiting portion on one side of the elastomeric structure causes bending around that layer (*16*). The slits allow for circumferential constraint while still allowing the gaps in between to stretch for actuation. Figure 1E shows that the finger curves in between the slits, yet there is negligible circumferential bulging. On the palm side of the actuators (i.e., the neutral bending plane), there was no elongation due to the solid sheet of nylon.

Control

For our demonstration, we used a single air supply for all four fingers and the thumb, and we used two solenoid valves (X-Valve, Parker Hannifin Corporation) for each finger to control actuation—one for allowing flow into a finger (actuate) and the other to exhaust it (deactuate). We controlled the on/off state of each valve to determine the pressure inside each finger and thus its motion. Although we have previously demonstrated sophisticated control over actuators (*16*, *43*), we chose "open loop" in this study to focus on the importance of the stretchable waveguides for active sensation. To test the capabilities of the prosthetic hand, we affixed it to the end joint of a 5-DOF robotic arm (CRS CataLyst Express; Fig. 3B).

Sensing

To impart the sense of touch to the soft prosthetic, we embedded the photonic strain sensors throughout the actuator membranes. In our demonstration, we incorporated three waveguides into each finger, where each finger is bent into a U-shape (toward the gravity-driven interface) so that LEDs can transmit light through the entirety of the actuators and the photodetectors can sense it on the other side (Fig. 1E). The photonic sensor located at the top of the actuator experiences the largest axial strain and thus the largest sensitivity to the bending motion. We placed the second sensor in the middle plane of the finger, which has medium axial strain and relays information about internal pressure.

The final waveguide serves as a touch sensor for the fingertip of the prosthetic hand; we achieve this isolated function by placing it at the neutral bending plane, where there is no axial strain. This photonic sensor is different from the other two sensors because it is longer and extends to the tip of the finger. The tip of the finger experiences no deformation while inflating and is used solely for detecting contact force when touching objects. To tune the external force sensing range of our prosthetic hand's fingertips, we integrated a stiff plate (ΔA ~ 2 mm × 3 mm) at the fingertips in contact with the waveguide to enhance the sensitivity (Fig. 3A). This force-amplifying structure directly transmits external tip force to the waveguide.

Movie S4 demonstrates the isolated functions of three waveguides in one finger: (i) when we pressed the fingertip, the bottom waveguide responded and the other two did not; (ii) when we inflated the finger, the middle and top waveguides immediately showed responses and the bottom waveguide did not. To distinguish the different functions of the middle and top waveguides, we kept the inflation pressure constant while straightening the finger back; we observed a notable signal drop (50%) for the top waveguide and a negligible signal drop (10%) for the middle waveguide. When the finger is deflated, there is a substantial signal drop (90%) for the middle waveguide. In the following section, we use these differences for haptic sensation.

Active haptic sensing experiments

Our soft prosthetic hand is a multifunctional one with both powerful motor (Fig. 4, A to C) and versatile sensory (Fig. 4, D to F) capabilities. Each digit of the hand is capable of both proprioception (sensing

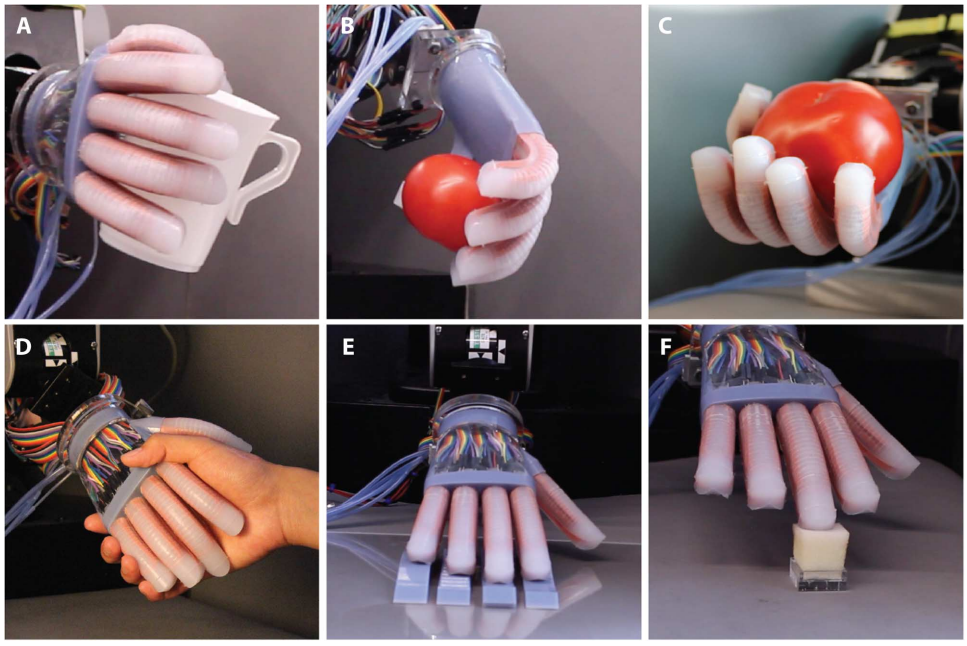

Fig. 4. Capabilities of the hand. (**A**) Holding a coffee mug; (**B** and **C**) grasping a tomato with the palm facing down (B) and the palm facing up (C); (**D**) shaking a human hand; (**E**) lateral scanning over surfaces to detect roughness and shape; and (**F**) probing the softness of a soft sponge using the middle finger.

internal pressure and active bending) and exteroception (sensing passive bending and external force at the fingertip). To demonstrate these capabilities, we designed three experiments inspired by common tasks of the human hand, including detecting shape and texture, probing softness, and object recognition.

Lateral scanning to detect shape and texture

The most commonly used exploratory procedure for detecting the roughness and shape of a surface by a human hand is lateral scanning (*44*). Using our robotic arm, we guided the hand to conduct lateral scans at a fixed height over several surfaces to distinguish their shape and texture (movie S5). We oriented the palm of the hand at a shallow angle (20°) with the surface so that each fingertip was touching the surface. When performing lateral scanning, the soft finger can be expressed as a spring and the height of the point it is touching changes the states of the spring—both compression distance (ΔH) and contact force (ΔF). As the fingers moved along the contoured surfaces, the bottom waveguide measured ΔF as it changed with surface height, ΔH. Increasing the stiffness of the finger also increases its sensitivity, $k = \Delta H/\Delta F$. As actuation pressure increases, the measurement sensitivity increases, but this increased pressure also causes the hand to close. With an actuator pressure of ΔP = 100 kPa (~15 psi), we were able to find a suitable balance between sensitivity and an open-hand shape.

Using this method, we tested the ability of the fingers to topographically map seven different 3D-printed surfaces (Fig. 5A, left). After a simple calibration using an inclined plane with known height and angle, we reconstructed the height profile of the seven surfaces (Fig. 5A, right). From these data, we observed that our prosthetic hand could distinguish curves as small as 5 m^{-1} and roughness on the order of 100 μm. We also found that our hand can be used to reconstruct the shape of simple objects such as a computer mouse (Fig. 5, C and D), including the scroll wheel and the click of the mouse buttons. Although the sensitivity of our hand is far from that of a human's, which can sense roughness on the scale of nanometers (*45*), we have demonstrated a promising system for replicating shape and texture detection using stretchable, optical sensors with a soft hand.

Softness detection

Along with shape and texture, our hands can also detect the softness of objects. Because the relationship between ΔH and ΔF is used in most forms of mechanical testing, we applied this information to measuring the softness of objects. To demonstrate this ability, we used our prosthetic hand to measure the softness of an unblocked (control) state, along with five common materials and objects: acrylic, polyurethane sponge, silicone rubber, a ripe tomato, and an unripe tomato. We measured their softness by positioning the tip of an unactuated (0 kPa) finger so that it was barely touching the top of the object to be measured. We took readings of the tip force and the degree of bending in the unactuated state as well as at varying internal pressures, indicated by the bottom waveguide power loss and the top waveguide power loss, respectively (movie S6).

Figure 6A shows the index finger measuring the softness of the unblocked state, sponge, and acrylic. The system, consisting of the finger and the material being probed, can be modeled as a two-spring system (Fig. 6B). By varying the stiffness of the finger (via the internal pressure, which is monitored by the middle waveguide power loss), we were able to generate a stress-strain curve for each of the materials we measured (Fig. 6C): The loss in the bottom waveguide is proportional to the contact force (thus stress) on the object, whereas the loss in the top waveguide is proportional to its deformation (thus strain). We measured four states (0, 33, 67, and 100 kPa) for each object and fit them into a linear curve. The slope of these fitted lines is the indicator we picked for the softness of the objects (larger slopes indicate harder objects). As expected, these data show the objects decreasing in softness in the following order: unblocked, sponge, rubber, ripe tomato,

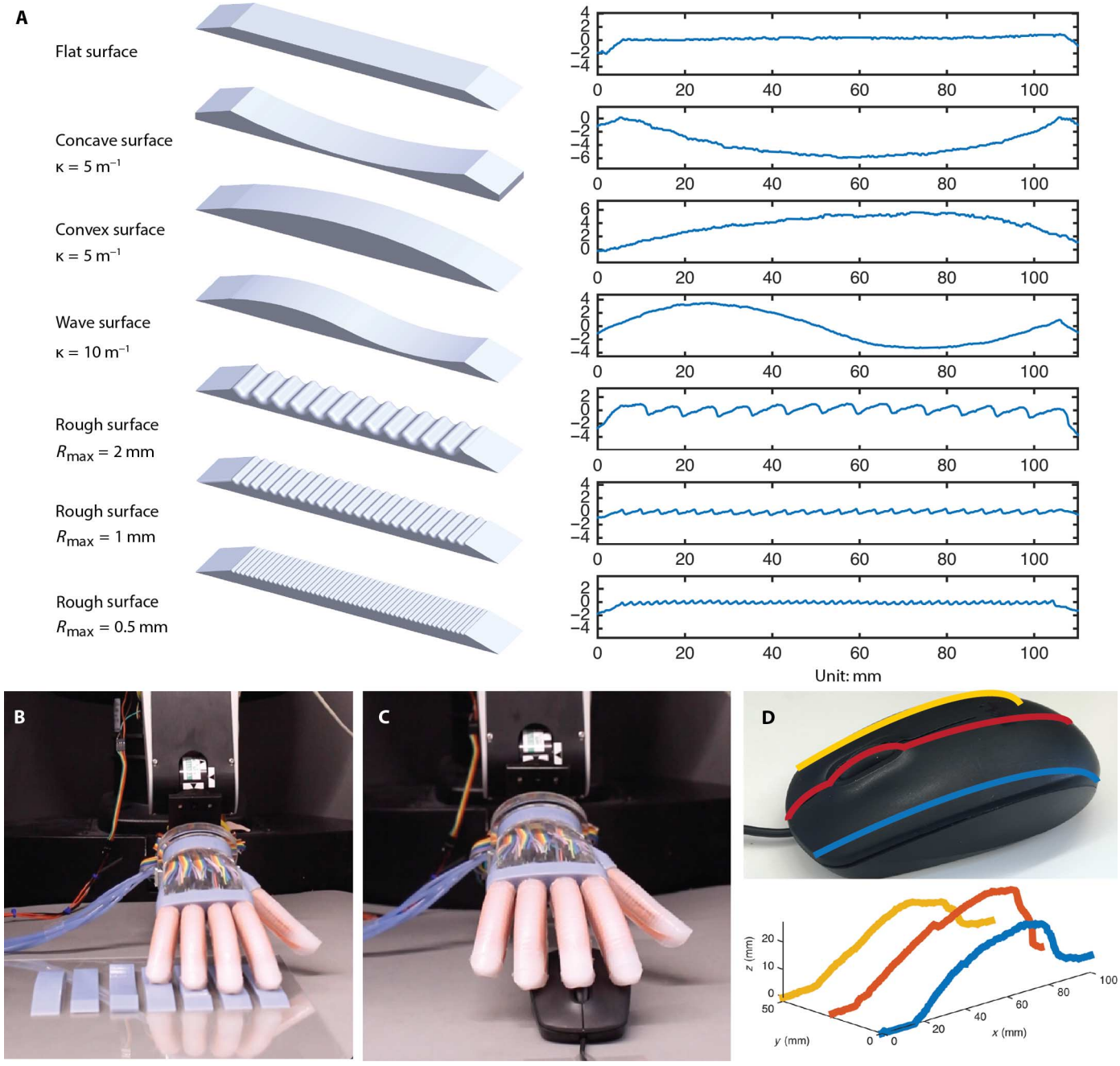

Fig. 5. Shape and texture detection. (**A**) Seven surfaces of different shape and roughness (left) and the reconstructed surfaces by the hand (right); (**B**) image of the lateral scanning for (A) using the bottom waveguide of each digit; (**C**) lateral scanning of a computer mouse; (**D**) mouse and the reconstructed shape.

unripe tomato, and acrylic. Note that our hand can barely distinguish the difference in softness between an unripe tomato and the acrylic. This issue is mainly attributable to the large contrast between the object's stiffness and that of the finger: Higher internal pressures would be required to achieve detectable position changes in harder objects. This result is similar to that of the human's process of detecting softness: We apply a large force to detect a hard object and a gentle press for a soft one.

Object recognition

In our final demonstration, we combined shape and softness measurement to select the ripest (softest) among a group of three tomatoes aligned in a row. First, we used our lateral-scanning, shape-reconstruction method to determine the shape and location of the three tomatoes (Fig. 7A). After determining their location, we positioned the index finger to measure their softness (Fig. 7B). As shown in movie S7, our hand was able to locate and select the ripe (red) tomato based on its softness. Although there is seemingly little difference in output signal from tomato 2 to tomato 3, we were still able to determine that the ripe tomato was softer (larger top waveguide loss and smaller bottom waveguide loss). During scanning and probing, our soft prosthetic hand executed a human-like gentle motion to avoid the risk of destroying the tomatoes.

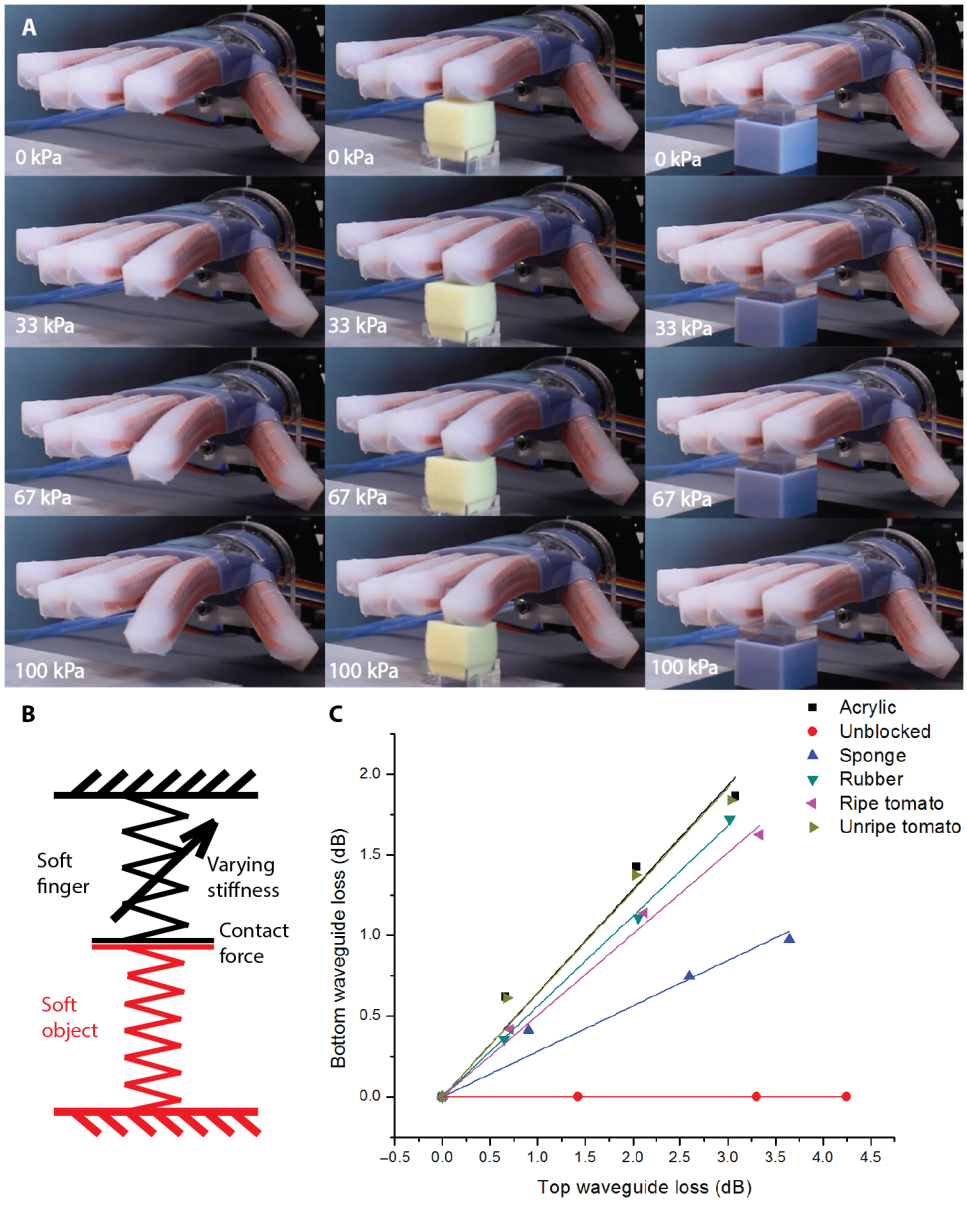

Fig. 6. Softness detection. (**A**) States of the softness detection at different air pressures for unblocked (left), sponge (middle), and acrylic (right); (**B**) model of softness detection; (**C**) force-curvature curves for different objects detected from the bottom and top waveguides of the index.

DISCUSSION

In this article, we presented a soft prosthetic hand with rich sensation realized via stretchable optical waveguides. Our work is the combination and extension of several developing areas in both materials science and robotics: 3D printing, soft lithography, and soft robotics. This sensor demonstrates excellent precision (a signal-to-noise ratio of >50) and stretchability ($\Delta\epsilon$ ~ 85% strain). We believe that the easy fabrication, low cost, chemical compatibility, and high repeatability of the developed stretchable waveguide sensors will benefit the field of robotics (e.g., soft robot bodies and skins for hard ones). In addition, we demonstrated that soft prosthetic hands could not only perform dexterous manipulation but also achieve various haptic sensing functions through simple innervation and control.

Our current prosthetic hand prototype, still in its early stage, shows many capabilities yet still has many aspects that can be improved on. First, sensory density can be greatly increased. Because the waveguide sensors and the body of the actuator share the same material library, more sensors could be incorporated into the actuators or completely replace the body of the actuators, to achieve higher information density for both proprioception and exteroception. The sensitivity can also be increased by using a larger power range from the LED (from the baseline power to ambient light power), by using high-power laser diodes, and by increasing the pressure range of the soft actuators (within the material's elasticity range) to press on objects with more force. In essence, the waveguide sensor we developed is a strain sensor based on geometric change; therefore, by 3D-printing more complex

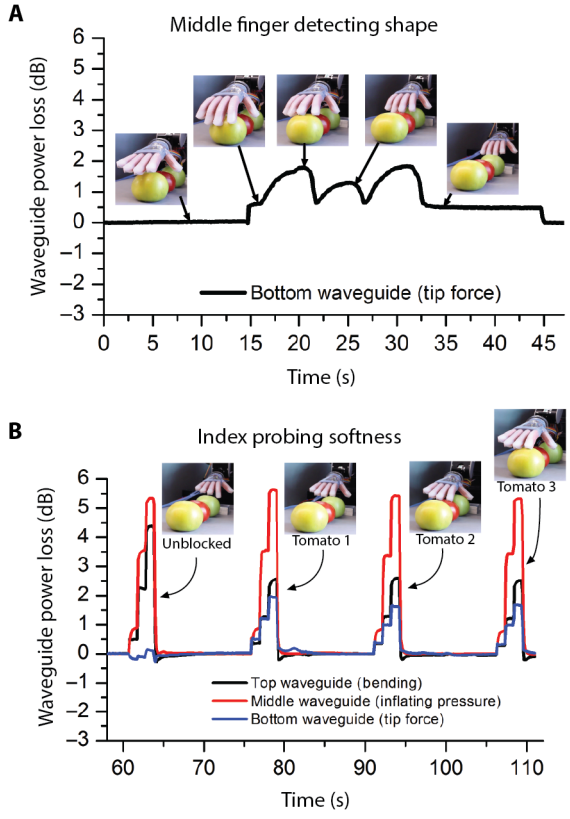

Fig. 7. Waveguide power loss during shape detection and probing softness. (**A**) Process of middle finger detecting the shape using its bottom waveguide: actuate fingers, scan above tomatoes, de-actuate fingers. (**B**) Process of index finger probing the softness using three waveguides: press unblocked, press tomato 1 (unripe), press tomato 2 (ripe), and press tomato 3 (unripe).

sensor shapes, sensors have uses other than bending, pressure, and press sensing (e.g., damage detection). Last, although we positioned these sensors in different places on the actuator, we still observed signal coupling. When more sensors are incorporated to extract denser information, the output signals will be increasingly coupled, and it will be difficult to calibrate the relationship between input and output signals; however, because the outputs of waveguide sensors are precise and repeatable, we could use machine-learning techniques to map inputs to outputs (regression) or perform more subtle object recognition (classification) by collecting large quantities of data (*46*).

MATERIALS AND METHODS

Objectives and design of the study

Our objective is to prove that optical sensors can be cointegrated into soft actuators and provide high-quality sensory capabilities. We designed an elastomeric optical waveguide that is highly stretchable, chemically stable, and easy to fabricate and that exhibits high precision in signal output. We chose the combination of 3D printing and soft lithography as the fabrication method because of its large design freedom and proven ability to replicate shapes in soft materials with high precision (*18*). We designed each finger of our prosthetic hand to be soft to make use of their intrinsic compliance so that we can implement most of our experiments by open-loop control. The softness of the finger actuators allows external forces to transmit to the internal structure and embedded sensors.

Fabrication of waveguides

Molds for cladding were 3D-printed using an Objet 3D printer in glossy mode. The mold was put in an oven at 60°C for 4 hours. Mold release was applied on the surface of the mold. ELASTOSIL M 4601 A/B were mixed at a ratio of 1:1 using a planetary centrifugal mixer at a speed of 2000 revolutions per minute (rpm) for 30 s, and the mixed pre-elastomer was poured into the mold for cladding and put in the oven at 60°C for 1 hour for curing. The cured piece was demolded from the mold and laid flat on a tray. VytaFlex 20 parts A and B were mixed at a ratio of 1:1 using a planetary centrifugal mixer at a speed of 2000 rpm for 1 min, and the mixed pre-elastomer was poured into the cured cladding piece within 10 min. The cladding with the uncured core was put on a hot plate at 70°C for 1 hour. After the core was cured, the pre-elastomer of M 4601 (prepared in the same way as the cladding piece) was poured onto the top of the core and cured in the oven.

Fabrication of the innervated finger

Two shorter waveguides and one longer waveguide were prepared in advance. Linear slits were cut into a rectangular piece of nylon fabric (see fig. S7). Three waveguides, the nylon fabric, and the finger molds (fig. S6) were assembled together, and the mold cap was put on. The pre-elastomer of Ecoflex 30 was poured into the mold. Last, a thin steel spring wire was inserted into the mold through a thin hole on the mold cap. The assembly was put in the oven at 60°C for 30 min. The assembly was disassembled, the steel wire was taken off, and the cured finger was demolded. A tube was inserted from the end hole, and a clamp was used to fasten the air inlet.

Characterization of materials

The refractive index of materials was measured using a Woollam spectroscopic ellipsometer with 30 mm × 30 mm × 3 mm samples. The absorbance of materials was measured using a Shimadzu UV-VIS-NIR spectrometer. The mechanical tests were conducted on a Zwick tensile test machine. Surface roughness was measured using a MicroXAM optical profilometer. Three separate samples were used to conduct each characterization.

Characterization methods for waveguide sensors

Elongation

We fixed two ends of the waveguide onto the two jaws of a bench vise and precisely rotated the screws to stretch the waveguide to different strains. At the same time, we recorded the power loss (fig. S4A).

Bending

We manipulated the waveguide to conform to laser-cut acrylic arcs and recorded the corresponding power loss (fig. S4B).

Pressing

We fixed the ends of the waveguide and laid it flat on a scale. We then put a plate with a known width onto the waveguide and placed different weights onto the plate to record the power loss. This process was repeated with plates of varying width (fig. S4C). Only one sample was used for each characterization, and each signal was collected 20 times to obtain the mean and SD.

Data acquisition and processing

We used an LED as the light source and a photodetector as the light sensor for our optical waveguides. Using a current-to-voltage (I/V) converter circuit (fig. S8), we were able to detect the light power received at the photodetector. Because of slight variations in manufacturing, some waveguides had higher intrinsic power loss than others. We selected the resistance values for our LED and I/V converter circuits to adjust for these differences in transmissivity between waveguides. With appropriate resistor values selected (table S1), each waveguide sensor produced a maximum voltage of about 5 V. By measuring the voltage, we determined the power loss of the sensors when stretched, bent, or touched. Capacitance in the I/V converter circuit was chosen to be 4700 pF to ensure low noise and high speed. We measured the output voltage of our circuits using 15 analog pins of an Arduino microcontroller (Arduino MEGA 2560) and used its serial port with a baud rate of 9600 to transmit the data to a computer. These data were received through MATLAB R2016 for further processing and plotting. Our sampling frequency was about 60 Hz for each of the 15 sensor channels.

SUPPLEMENTARY MATERIALS

robotics.sciencemag.org/cgi/content/full/1/1/eaai7529/DC1
Fig. S1. Optical properties of M 4601 A/B, Ecoflex 30, and VytaFlex 20.
Fig. S2. Mechanical properties of M 4601 A/B, Ecoflex 30, and VytaFlex 20.
Fig. S3. Surface profile of waveguide core/cladding interfaces.
Fig. S4. Characterization setups.
Fig. S5. Repeatability tests.
Fig. S6. Mold design for the middle finger.
Fig. S7. Nylon fabric and mold assembly.
Fig. S8. Circuit for powering LED and amplifying photodiode current.
Table S1. Resistors and capacitors used in LED-photodiode circuits for waveguide.
Movie S1. Elongation sensor characterization.
Movie S2. Bending sensor characterization.
Movie S3. Pressure sensor characterization.
Movie S4. Decoupling signals from three waveguide sensors in one finger.
Movie S5. Lateral scanning to detect texture and shape.
Movie S6. Pressing to detect softness.
Movie S7. Object recognition.

REFERENCES AND NOTES

1. L. A. Jones, S. J. Lederman, *Human Hand Function* (Oxford Univ. Press, 2006).
2. M. C. Carrozza, B. Massa, S. Micera, R. Lazzarini, M. Zecca, P. Dario, The development of a novel prosthetic hand—Ongoing research and preliminary results. *IEEE ASME T. Mech.* **7**, 108–114 (2002).
3. M. A. Lebedev, M. A. L. Nicolelis, Brain–machine interfaces: Past, present and future. *Trends Neurosci.* **29**, 536–546 (2006).
4. P. M. Rossini, S. Micera, A. Benvenuto, J. Carpaneto, G. Cavallo, L. Citi, C. Cipriani, L. Denaro, V. Denaro, G. Di Pino, F. Ferreri, E. Guglielmelli, K.-P. Hoffmann, S. Raspopovic, J. Rigosa, L. Rossini, M. Tombini, P. Dario, Double nerve intraneural interface implant on a human amputee for robotic hand control. *Clin. Neurophysiol.* **121**, 777–783 (2010).
5. G. A. Tabot, J. F. Dammann, J. A. Berg, F. V Tenore, J. L. Boback, R. J. Vogelstein, S. J. Bensmaia, Restoring the sense of touch with a prosthetic hand through a brain interface. *Proc. Natl. Acad. Sci. U.S.A.* **111**, 875 (2013).
6. G. S. Dhillon, K. W. Horch, Direct neural sensory feedback and control of a prosthetic arm. *IEEE Trans. Neural Syst. Rehabil. Eng.* **13**, 468–472 (2005).
7. S. Raspopovic, M. Capogrosso, F. M. Petrini, M. Bonizzato, J. Rigosa, G. Di Pino, M. Controzzi, T. Boretius, E. Fernandez, G. Granata, C. M. Oddo, A. L. Ciancio, C. Cipriani, M. C. Carrozza, W. Jensen, E. Guglielmelli, T. Stieglitz, P. M. Rossini, S. Micera, Restoring natural sensory feedback in real-time bidirectional hand prostheses. *Sci. Transl. Med.* **6**, 222ra19 (2014).
8. T. Mouri, H. Kawasaki, K. Yoshikawa, J. Takai, S. Ito, Anthropomorphic robot hand: Gifu hand II, in *Proceedings of the 2002 International Conference on Control, Automation and Systems (ICCAS 2002)* (Institute of Control, Automation and Systems Engineers, 2002), pp. 1288–1293.
9. F. Röthling, R. Haschke, J. J. Steil, H. Ritter, Platform portable anthropomorphic grasping with the bielefeld 20-DOF shadow and 9-DOF TUM hand, in *Proceedings of the 2007 IEEE International Conference on Intelligent Robots and Systems (IROS)* (IEEE, 2007), pp. 2951–2956.
10. M. C. Carrozza, G. Cappiello, S. Micera, B. B. Edin, L. Beccai, C. Cipriani, Design of a cybernetic hand for perception and action. *Biol. Cybern.* **95**, 629–644 (2006).
11. A. D. Deshpande, Z. Xu, M. J. Vande Weghe, B. H. Brown, J. Ko, L. Y. Chang, D. D. Wilkinson, S. M. Bidic, Y. Matsuoka, Mechanisms of the anatomically correct testbed hand. *IEEE ASME T. Mech.* **18**, 238–250 (2013).
12. A. M. Dollar, R. D. Howe, The highly adaptive SDM hand: Design and performance evaluation. *Int. J. Robot. Res.* **29**, 585–597 (2010).
13. M. G. Catalano, G. Grioli, E. Farnioli, A. Serio, C. Piazza, A. Bicchi, Adaptive synergies for the design and control of the Pisa/IIT SoftHand. *Int. J. Robot. Res.* **33**, 768–782 (2014).
14. R. Deimel, O. Brock, A novel type of compliant and underactuated robotic hand for dexterous grasping. *Int. J. Robot. Res.* **35**, 161–185 (2016).
15. P. Polygerinos, K. Galloway, S. Sanan, M. Herman, C. J. Walsh, EMG controlled soft robotic glove for assistance during activities of daily living, in *Proceedings of the 14th IEEE/RAS-EMBS International Conference on Rehabilitation Robotics (ICORR 2015)* (IEEE, 2015), pp. 55–60.
16. H. Zhao, J. Jalving, R. Huang, R. Knepper, A. Ruina, R. Shepherd, A helping hand: Soft orthosis with integrated optical strain sensors and EMG control. *IEEE Robot. Autom. Mag.* **23**, 55–64 (2016).
17. A. Stilli, H. A. Wurdemann, K. Althoefer, Shrinkable, stiffness-controlled soft manipulator based on a bio-inspired antagonistic actuation principle, in *Proceedings of the 2014 IEEE/RSJ International Conference on Intelligent Robots and Systems (IROS 2014)* (IEEE, 2014), pp. 2476–2481.
18. R. F. Shepherd, F. Illievski, W. Choi, S. A. Morin, A. A. Stokes, A. D. Mazzeo, X. Chen, M. Wang, G. M. Whitesides, Multigait soft robot. *Proc. Natl. Acad. Sci. U.S A.* **108**, 20400–20403 (2011).
19. F. Ilievski, A. D. Mazzeo, R. F. Shepherd, X. Chen, G. M. Whitesides, Soft robotics for chemists. *Angew. Chem. Int. Ed.* **50**, 1890–1895 (2011).
20. H. Zhao, Y. Li, A. Elsamadisi, R. Shepherd, Scalable manufacturing of high force wearable soft actuators. *Extreme Mech. Lett.* **3**, 89–104 (2015).
21. A. D. Marchese, R. K. Katzschmann, D. Rus, A recipe for soft fluidic elastomer robots. *Soft Robot.* **2**, 7–25 (2015).
22. B. N. Peele, T. J. Wallin, H. Zhao, R. F. Shepherd, 3D printing antagonistic systems of artificial muscle using projection stereolithography. *Bioinspir. Biomim.* **10**, 055003 (2015).
23. S. S. Robinson, K. W. O'Brien, H. Zhao, B. N. Peele, C. M. Larson, B. C. Mac Murray, I. M. Van Meerbeek, S. N. Dunham, R. F. Shepherd, Integrated soft sensors and elastomeric actuators for tactile machines with kinesthetic sense. *Extreme Mech. Lett.* **5**, 47–53 (2015).
24. C. Larson, B. Peele, S. Li, S. Robinson, M. Totaro, L. Beccai, B. Mazzolai, R. Shepherd, Highly stretchable electroluminescent skin for optical signaling and tactile sensing. *Science* **351**, 1071–1074 (2016).
25. M. Amjadi, K.-U. Kyung, I. Park, M. Sitti, Stretchable, skin-mountable, and wearable strain sensors and their potential applications: A review. *Adv. Funct. Mater.* **26**, 1678–1698 (2016).
26. C. To, T. L. Hellebrekers, Y.-L. Park, Highly stretchable optical sensors for pressure, strain, and curvature measurement, in *Proceedings of the 2015 IEEE/RSJ International Conference on Intelligent Robots and Systems (IROS)* (IEEE, 2015), pp. 5898–5903.
27. F. L. Hammond, Y. Mengüc, R. J. Wood, Toward a modular soft sensor-embedded glove for human hand motion and tactile pressure measurement, in *Proceedings of the 2014 IEEE/RSJ International Conference on Intelligent Robots and Systems (IROS 2014)* (IEEE, 2014), pp. 4000–4007.
28. L. P. Jentoft, A. M. Dollar, C. R. Wagner, R. D. Howe, Intrinsic embedded sensors for polymeric mechatronics: Flexure and force sensing. *Sensors* **14**, 3861–3870 (2014).
29. H. A. Wurdemann, S. Sareh, A. Shafti, Y. Noh, A. Faragasso, D. S. Chathuranga, H. Liu, S. Hirai, Embedded electro-conductive yarn for shape sensing of soft robotic manipulators. *Conf. Proc. IEEE Eng. Med. Biol. Soc.* **2015**, 8026–8029 (2015).
30. J. Maher, "Waveguide optical modulator," U.S. Patent 4,128,299 (1978).
31. Y. Shibata, A. Nishimura, S. Niwa, Y. Osawa, T. Uemiya, "Optical sensors," U.S. Patent 4,750,796 (1988).
32. S. Begej, Planar and finger-shaped optical tactile sensors for robotic applications. *IEEE Trans. Robot. Autom.* **4**, 472–484 (1988).
33. G. J. Kookootsedes, H. H. Reese, B. I. Gutek, G. H. Pretzer, "Touch position sensitive optical waveguides," U.S. Patent 4,701,017 (1987).
34. N. Lagakos, E. U. Schnaus, H. H. Cole, J. Jarzynski, J. A. Bucaro, Optimizing fiber coatings for interferometric acoustic sensors. *IEEE Trans. Microw. Theory Tech.* **30**, 529–535 (1982).
35. R. A. Lieberman, L. L. Blyler, L. G. Cohen, A distributed fiber optic sensor based on cladding fluorescence. *J. Lightwave Technol.* **8**, 212–220 (1990).

36. O. J. A. Schueller, X.-M. Zhao, G. M. Whitesides, S. P. Smith, M. Prentiss, Fabrication of liquid-core waveguides by soft lithography. *Adv. Mater.* **11**, 37–41 (1999).
37. M. Ramuz, B. C.-K. Tee, J. B.-H. Tok, Z. Bao, Transparent, optical, pressure-sensitive artificial skin for large-area stretchable electronics. *Adv. Mater.* **24**, 3223–3227 (2012).
38. J. Missinne, S. Kalathimekkad, B. Van Hoe, E. Bosman, J. Vanfleteren, G. Van Streenberge, Stretchable optical waveguides. *Opt. Express* **22**, 4168–4179 (2014).
39. G. M. Whitesides, S. K. Y. Tang, Fluidic optics, in *Proceedings of the SPIE* (SPIE, 2006), pp. 1–13.
40. D. Qin, Y. Xia, G. M. Whitesides, Soft lithography for micro- and nanoscale patterning. *Nat. Protoc.* **5**, 491–502 (2010).
41. J. A. Jay, "An overview of macrobending and microbending of optical fibers," http://corning.com/media/worldwide/coc/documents/Fiber/RC-%20White%20Papers/WP-General/WP1212_12-10.pdf.
42. D. Rus, M. T. Tolley, Design, fabrication and control of soft robots. *Nature* **521**, 467–475 (2015).
43. H. Zhao, R. Huang, R. F. Shepherd, Curvature control of soft orthotics via low cost solid-state optics, in *Proceedings of the 2016 IEEE International Conference on Robotics and Automation (ICRA 2016)* (IEEE, 2016), pp. 4008–4013.
44. S. J. Lederman, R. L. Klatzky, Hand movements: A window into haptic object recognition. *Cogn. Psychol.* **19**, 342–368 (1987).
45. L. Skedung, M. Arvidsson, J. Y. Chung, C. M. Stafford, B. Berglund, M. W. Rutland, Feeling small: Exploring the tactile perception limits. *Sci. Rep.* **3**, 2617 (2013).
46. J. Gafford, F. Doshi-Velez, R. Wood, C. Walsh, Machine learning approaches to environmental disturbance rejection in multi-axis optoelectronic force sensors. *Sensor. Actuat. A Phys.* **248**, 78–87 (2016).

Acknowledgments: We thank A. Ruina for input on the soft finger design. We also thank our group mates B. Peele, C. Larson, and J. Pikul for support and help during the experiments. **Funding:** This work was supported by the Air Force Office of Scientific Research under award number FA9550-15-1-0160. Part of the study was performed at the Cornell NanoScale Facility, a member of the National Nanotechnology Coordinated Infrastructure, which was supported by the NSF (grant ECCS-1542081), and the Cornell Center for Materials Research Shared Facilities, which was supported through the NSF Materials Research Science and Engineering Centers program (DMR-1120296). **Author contributions:** H.Z. fabricated the waveguides and the prosthetic hand, designed the experiments, conducted the experiments, analyzed the data, and wrote the manuscript; K.O. designed and built the current amplifying circuits, conducted the experiments, and edited the manuscript; S.L. conducted the material characterization and edited the manuscript; R.F.S. initialized the concept, designed the experiments, supervised the experiments, and wrote the manuscript. **Competing interests:** R.F.S. and H.Z. are inventors on a patent application (no. 62/382,484) submitted by Cornell University that covers stretchable waveguide fabrication. The remaining authors declare that they have no competing interests. **Data and materials availability:** Contact R.F.S. for any questions regarding experimental raw data and design schematics.

Submitted 7 August 2016
Accepted 19 October 2016
Published 6 December 2016
10.1126/scirobotics.aai7529

Citation: H. Zhao, K. O'Brien, S. Li, R. F. Shepherd, Optoelectronically innervated soft prosthetic hand via stretchable optical waveguides. *Sci. Robot.* **1**, eaai7529 (2016).

Science Robotics

Optoelectronically innervated soft prosthetic hand via stretchable optical waveguides

Huichan Zhao, Kevin O'Brien, Shuo Li, and Robert F. Shepherd

Sci. Robot. **1** (1), eaai7529. DOI: 10.1126/scirobotics.aai7529

Science Robotics (ISSN 2470-9476) is published by the American Association for the Advancement of Science. 1200 New York Avenue NW, Washington, DC 20005. The title *Science Robotics* is a registered trademark of AAAS.